# Combined effects of precipitation anomalies and dams on streamwater-groundwater interaction in the Fen River basin, China

Science of the Total Environment

Xia, Yun; Xiao, Jun; van der Ploeg, Martine; Wang, Wanzhou; Li, Zhi

https://doi.org/10.1016/j.scitotenv.2024.172704

Science of the Total Environment 929 (2024) 172704

Contents lists available at ScienceDirect

Science of the Total Environment

journal homepage: www.elsevier.com/locate/scitotenv

# Combined effects of precipitation anomalies and dams on streamwater-groundwater interaction in the Fen River basin, China

Yun Xia [a], Jun Xiao [b,*], Martine van der Ploeg [c], Wanzhou Wang [a], Zhi Li [a,*]

[a] State Key Laboratory of Soil Erosion and Dryland Farming on the Loess Plateau, College of Natural Resources and Environment, Northwest A&F University, Yangling, Shaanxi 712100, China
[b] State Key Laboratory of Loess and Quaternary Geology, Institute of Earth Environment, Chinese Academy of Sciences, Xi'an, Shaanxi 710061, China
[c] Hydrology and Environmental Hydraulics Group, Wageningen University, Wageningen, the Netherlands

## HIGHLIGHTS

- Damming and precipitation anomalies jointly influence the dynamics of SGI.
- Dams reversed SGI, boosting streamwater infiltration ratios from 0 to 29 % to 78 %.
- Groundwater discharge is impeded in front of the dam but facilitated behind.
- Precipitation anomalies notably magnify interannual variations in SGI patterns.

## GRAPHICAL ABSTRACT

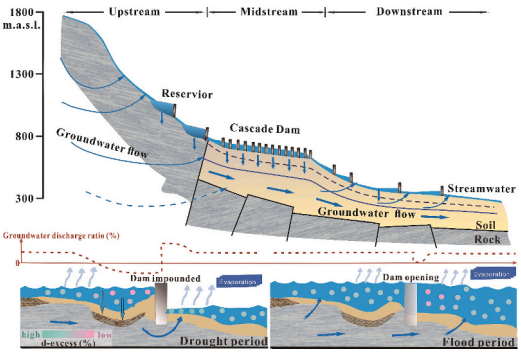


## ARTICLE INFO

Editor: Christian Herrera

*Keywords:*
Dam regulation
Precipitation anomalies
Streamwater-groundwater interactions
Tracer methods
Combine effect

## ABSTRACT

Both water management measures like damming and changes in precipitation as a result of anthropogenic induced climate change have exerted profound effects on the dynamics of streamwater-groundwater interaction (SGI). However, their compound effects on SGI have not been investigated so far. Taking the Fen River of China as an example, this study aims to examine the synergistic impacts of damming and precipitation anomalies on SGI dynamics. The sampling considered the seasonal and interannual variability of precipitation (May and September in 2019 representing a dry year; May and August in 2021 representing a wet year), and long-term daily observational data, including water levels and water discharge, were combined to elucidate the compound effects. Precipitation anomalies and damming exert significant individual and combined influences on SGI. Separately, dams and reservoirs reversed the SGI dynamics, significantly increasing the contributions of streamwater to groundwater from 0 to 29 % to 78 % in the dam-affected areas. Further, the groundwater discharge ratios behind the dam (about 60 %) were three times higher than those in front of the dam. Precipitation anomalies significantly amplified interannual variability in SGI patterns, and groundwater discharge ratios increased by 47 % during the dry period (2019) compared to flood period (2021). The combined influence of precipitation anomalies and dam regulation remarkably changed the lateral, vertical, and longitudinal water exchange dynamics. Precipitation anomalies affected the SGI dynamics at the whole watershed scale, whereas

* Corresponding authors.
*E-mail addresses:* xiaojun@ieecas.cn (J. Xiao), lizhibox@126.com (Z. Li).

https://doi.org/10.1016/j.scitotenv.2024.172704
Received 20 February 2024; Received in revised form 20 April 2024; Accepted 21 April 2024
Available online 23 April 2024

dam regulation regimes exhibited a stronger control at the local scale. The compound effects of dam regulation and precipitation anomalies can result in different SGI patterns under various climate scenarios. More attention should be paid to the interrelated feedback mechanisms between damming, extreme precipitation events, and their impact on the watershed-scale hydrological cycle.

## 1. Introduction

Streamwater and groundwater hydraulically interact (SGI) through vertical, lateral, and longitudinal water flows, and the interaction significantly influences the water-related issues such as over-allocation, aquifer salinity, and environmental flows (Boulton et al., 2017; Yuan et al., 2020). Comprehensively understanding and quantifying SGI are vital for the sustainable development of collaborative water management and eco-environmental protection (Wang et al., 2022; Yang et al., 2021). However, SGI exhibit strong spatial-temporal heterogeneity due to factors such as complex geomorphic conditions (Song et al., 2019), hydraulic gradients (Unland et al., 2013), water flow patterns (Malzone et al., 2016), and precipitation regimes (Dudley-Southern and Binley, 2015). In particular, the global climate change and intensive human activities such as hydraulic construction have further resulted in more complex, frequent, and drastic changes in SGI patterns (Guevara-Ochoa et al., 2020; Miao et al., 2020). Understanding how environmental factors and human activities influence SGI is therefore essential.

Approximately 2.8 million dams and reservoirs constructed worldwide over the past century, serving multiple purposes such as agricultural irrigation, drinking water supply, navigation, flood control, and hydropower generation (Grill et al., 2019). This significantly aggravates the complexity of SGI alterations. Especially, in densely-populated areas, rivers are heavily regulated, resulting in hydrological modifications including river discontinuity, flow regime changes, water level fluctuations, and sedimentation (Kondolf et al., 2014; Latrubesse et al., 2017; Wang et al., 2019), which increases the spatial-temporal heterogeneity of SGI. Moreover, the Intergovernmental Panel on Climate Change (IPCC, 2021) has reported an increase in the frequency and intensity of extreme climate events (e.g., drought and flood), further contributing to the uncertainties in identifying SGI (Fuchs et al., 2019; Geris et al., 2022). Specifically, droughts reduce regional precipitation and increase evaporation, significantly affecting water levels in both streamwater and groundwater (Fuchs et al., 2019; Jiang et al., 2021; Wu et al., 2022). Conversely, intense rainfall and flooding events can enhance groundwater recharge by expanding recharge zones and facilitating lateral transfer from the channel to the riparian areas (Dey et al., 2022; Geris et al., 2022).

Although extensive research has focused on the individual impacts of extreme climate events or damming on SGI (Francis et al., 2010; Geris et al., 2022), the synergistic effects of these factors on SGI dynamics remain underexplored, highlighting a critical gap our study aims to address. Moreover, previous studies mainly focused on the longer-term temporal variations in SGI dynamics, for example, before and after dam construction (Wang et al., 2021), overlooking the detailed description and change of the spatiotemporal dynamics of SGI under various dam management strategies corresponding to different precipitation regimes. Therefore, a comprehensive assessment of the coupled impact of precipitation anomalies and dam operation on SGI dynamic adds insight for integrated water resources management.

To elucidate SGI, researchers have employed multiple methodologies, including hydraulic methods (Partington et al., 2020), environmental tracers (e.g. hydrochemical and isotopic indicators) (Frei et al., 2020), heat tracing methods (Coutino et al., 2020), numerical modeling (Jutebring Sterte et al., 2018) as well as microbial community analysis (Li et al., 2023). However, few methods can be integrated with studying the effects of multiple influencing factors. Numerical modeling, for instance, can be employed to assess various anthropic pressure and climate change scenarios, but is more likely to be constrained by data availability and parameter selection (Martínez-Santos et al., 2010; Yan et al., 2023; Zaremehrjardy et al., 2022). Tracer-based methods are powerful in this matter—not only to characterize water cycles dynamics (e.g. groundwater recharge ratios and water evaporation) from point to regional scale (Geris et al., 2022; Wang et al., 2023a; Xia et al., 2024), but also provide insights into flow alterations resulting from precipitation anomalies (Jiang et al., 2022; King et al., 2015) and dam regulation (Geris et al., 2022; Zhou and Zhou, 2023). The combination of different tracers such as isotopic tracers and hydrochemical indicators, can provide complementary information, enhancing the accuracy of identifying water exchange processes (Herrera et al., 2023; Modie et al., 2022).

Taking the Fen River Basin (FRB) in China as an example study area to investigate the compound effects of water management and precipitation anomalies, we captured two hydrological years characterized by anomalous precipitation events and conducted four sampling periods encompassing both dry and wet seasons. Employing multi-tracer methods (i.e., main ion chemicals, δD, $\delta^{18}O$, d-excess), this study aims to (a) qualitatively and quantitatively identify the basin-scale spatiotemporal variations of SGI, (b) investigate the combined effects of precipitation anomalies and river damming on SGI.

## 2. Data and methods

### 2.1. Study area

The FRB (110.3°E−113.3°E, 35.2°N−39.0°N) is the Yellow River's second-largest primary tributary, covering a drainage area of 39,721 $km^2$ and extending over 713 km in length (Fig. 1a). The FRB has faced significant groundwater level declines due to prolonged excessive extraction (Shen et al., 2022). In response, water conservancy projects, including the establishment of 15 cascade dams in the middle reaches in 2017 (Fig. 1b), have been implemented to support groundwater recovery and rebalance water resources (Shen et al., 2022). To date, three large reservoirs (with a storage capacity of over 100 million $m^3$) and tens of medium-sized reservoirs, individual and cascade dams are scattered in the FRB.

The FRB transitions from semiarid to subhumid climates, with average annual temperatures ranging from 8.6 to 14.1 °C and an average annual precipitation of 440.2 mm—70 % of which falls from July to September. The elevation decreases from north to south, dividing into the upper, middle, and lower reaches by the Lancun and Shitan hydrographic stations (Xiao et al., 2021) (Fig. 1c). Land use predominantly consists of forestland upstream and cropland downstream, with significant groundwater reliance due to insufficient streamwater production. The main types of phreatic groundwater include pore water stored in Quaternary loose deposits and fracture water in clastic rock and karst water in carbonate rock (Fig. 1c). Notably, the Cambrian-Ordovician karstic aquifer, covering 87 % of the area, is a crucial groundwater source (Shen et al., 2022).

In 2019, the FRB experienced a severe drought due to El Niño, with precipitation falling 25 % below the annual average (Fig. S1). In contrast, 2021 witnessed a 43.5 % increase in precipitation attributed to double La Niña events (Fig. S1), significantly influencing water management strategies. During the dry year, water was conserved within dam/reservoirs, while dams prompted more discharges for flood control during the wet year. Therefore, the sampling campaigns were conducted during the dry and flood seasons in 2019 and 2021 to reveal the impacts of precipitation anomalies and dam regulation on SGI dynamics.

### 2.2. Sampling and analysis

A total of 201 streamwater and 165 groundwater samples were collected across two hydrological years, specifically in May and September of 2019, and May and August of 2021 (Fig. 1). Streamwater was sampled from the central point of water flow, positioned 0.5 m below the water surface. Groundwater samples, primarily collected within a 5 km radius of river sampling points, were drawn after over half an hour pumping to ensure representativeness. All the groundwater sampling wells had depths of <50 m. The water temperature (°C), pH, total dissolved solid (TDS) and electrical conductivity (EC, μS/cm) were measured in situ using a portable multi-parameter instrument (SG78-FK-CN, METTLER TOLEDO). Samples were immediately filtered through a 0.22 μm Whatman® nylon filter after collection, and the filtrate was divided into two 100 mL polyethylene bottles. One bottle was used for bicarbonate titration within 12 h. All water samples were refrigerated at 4 °C until measurement.

The concentrations of $HCO_3^-$ and $CO_3^{2-}$ were analyzed three times via acid-base titration with standard deviations <5 %. The anions and cations were analyzed using ion chromatography (DIONEX ICS-1100, Thermal Fisher Scientific, USA) and inductively coupled plasma-atomic emission spectrometry (ICP-6300), respectively. Both analyzers had an error < 1.5 %. Standard samples were introduced at intervals of twenty. The hydrogen and oxygen isotope compositions (δD and $\delta^{18}O$) of water samples were characterized with a liquid water isotope analyzer (LGR GLA431-TLWIA, ABB Inc., Canada) with the analytical precision of ±0.3 ‰ for δD and ±0.1 ‰ for $\delta^{18}O$, which measures each sample six times and averages the last four results.

### 2.3. Conceptual model and data analysis

To identify the individual and combined effects of precipitation anomalies and damming on SGI, our hypothesis assumes that during drought, diminished precipitation and damming combinedly increase river water infiltration. Conversely, in flood periods, the effects of dam impoundment and increased precipitation on SGI may diverge, leading to complex interactions characterized by increased groundwater discharge into the river in areas without dams and increased river infiltration occurring in the vicinity of dams. Spatially, the assumption is that the impact of dam construction within dammed regions is more pronounced than that of precipitation anomalies. The conceptual model of this study is shown in Fig. 2. To validate our hypothesis, we implement a three-step analysis: (1) qualitative and quantitative determination of SGI across different sampling periods; (2) comparison of SGI under varying precipitation and damming scenarios; (3) examination of their combined effect on SGI.

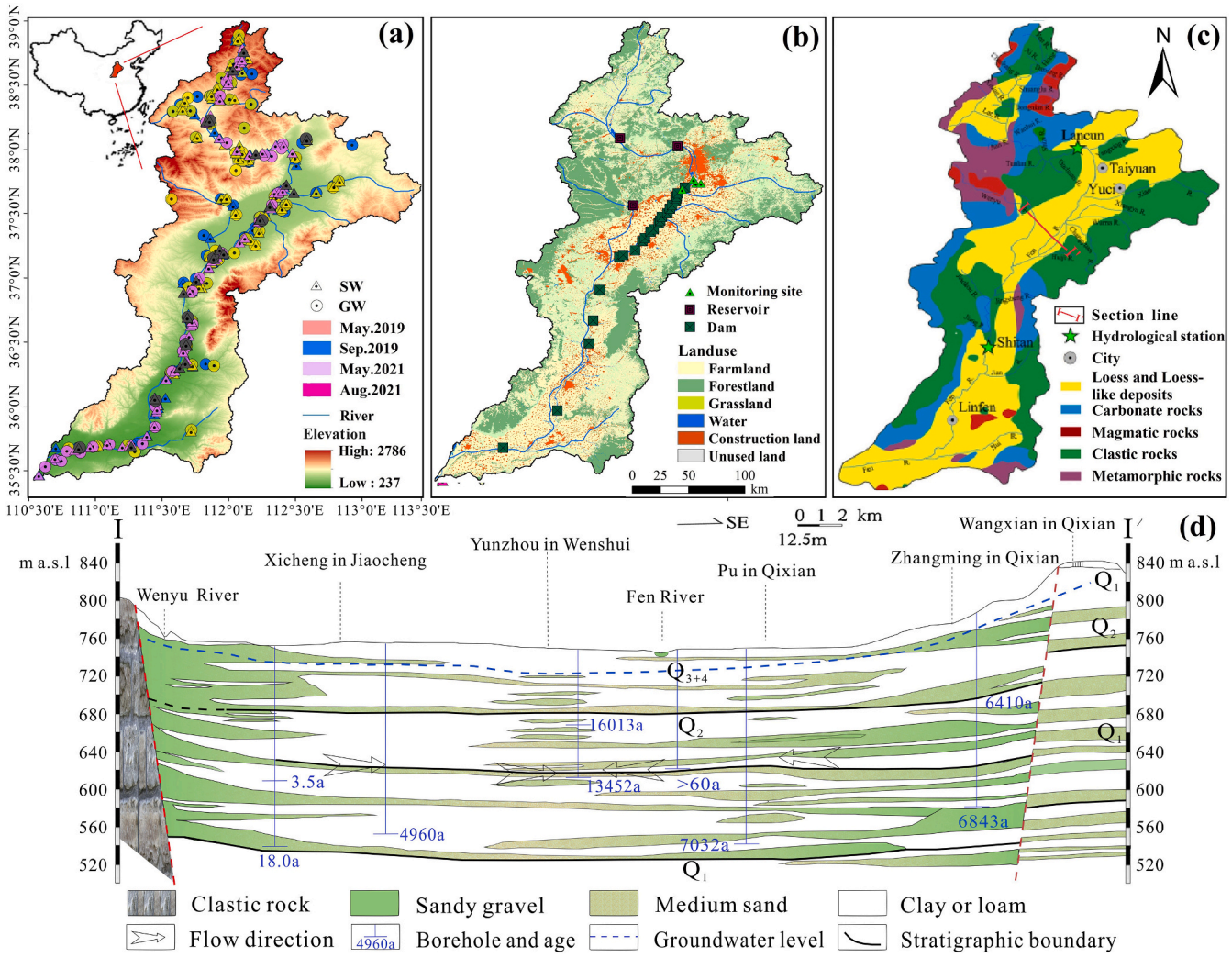


**Fig. 1.** Sampling location and hydrogeological characteristics. a) Elevation above sea level (a.s.l) and streamwater (SW) and groundwater (GW) sampling sites, b) land use type and groundwater monitoring sites, reservoirs, and dams, c) hydrogeology characteristics, and d) hydrogeological cross section along the I–I′ line and groundwater ages, modified from Guo et al. (2019).

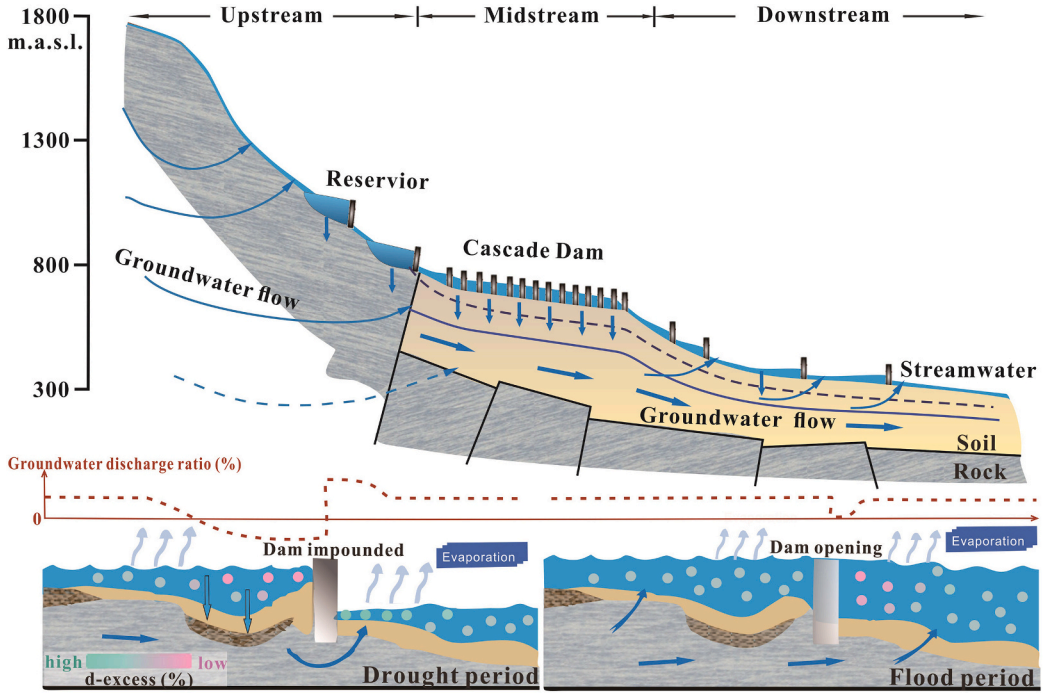


**Fig. 2.** Conceptual model elucidating the SGI dynamics under the combined effect of precipitation anomalies and damming.

For SGI identification, our analysis hinged on key principles: i) dual isotope plots, the intersection between the evaporation line (EL) and local meteoric water line (LMWL) delineates the isotopic composition of the input water. EL and LMWL refer to the linear relationships observed in isotopic compositions of groundwater/streamwater and precipitation, respectively. These relationships aid in interpreting the isotopic composition of water samples and understanding processes such as water origins, evaporation, and mixing (Xie et al., 2024; Yapiyev et al., 2023). ii) the variations of $\delta^{18}O$, $Cl^-$, and deuterium excess (d-excess = $\delta^2H - 8 \times \delta^{18}O$) values in paired streamwater and groundwater samples along the river flow paths. The d-excess values, representing the deviation of local precipitation samples from the Global Meteoric Water Line (Wu et al., 2018), offer insights into evaporation intensity and kinetic fractionation effects, serving as a complementary indicator for studying hydrological processes like water exchange and recharge (Hu et al., 2023; Qu et al., 2023; Wang et al., 2023b). iii) the source-sink theory, where sinks typically accumulate solutes and exhibit higher ion concentrations (Kendall and Doctor, 2003; Li et al., 2017). Hierarchical Cluster Analysis (HCA) was used to classify water samples with similar hydrochemical phases, enabling a detailed exploration of hydrochemical evolution processes and the dynamics of SGI in line with the source-sink theory (Guggenmos et al., 2011). The parameters applied for the HCA included EC, pH, $Ca^{2+}$, $Mg^{2+}$, $K^+$, $Na^+$, $Cl^-$, $SO_4^{2-}$, $HCO_3^-$ and $NO_3^-$.

To quantify SGI exchange ratios, we utilized the Bayesian Stable Isotope model (Mix SIAR version 3.1), which is supported by R graphical user package (more details in (Parnell et al., 2010)). Isotopic ($\delta D$-$\delta^{18}O$) and hydrochemical (EC-$Cl^-$) indicators were employed in the model to estimate SGI exchange ratios. A significant positive correlation ($p < 0.01$) was observed between the results of these two indicator-combinations, and the average contributions were used for further analysis to reduce uncertainties. The detailed steps for identifying SGI were provided in the supplementary materials (Fig. S2). In order to understand the combined impacts of precipitation anomalies and damming on SGI, we compared the relationship between SGI and precipitation across various sampling periods, and further conducted a detailed spatial analysis of the dam's influence on the laterally, vertically, and longitudinally water exchange dynamics.

Moreover, the Gibbs diagram was used to analyze the dominant geochemical processes (i.e., rock weathering, evaporation and precipitation) controlling water chemistry (Gibbs, 1970). The spatiotemporal variations of isotopic and hydrochemical parameters in streamwater and groundwater were analyzed by nonparametric tests. Correlation analysis was used to characterize the relationships between groundwater discharge ratios and impact factors, e.g., dam density and distance.

### 2.4. Hydrometeorological data

The identification of drought or abundant years in the FRB was based on the average annual precipitation amount at the Taiyuan meteorological stations from 1980 to 2021 (http://data.cma.cn/). The groundwater level data from 2017 to 2021 were obtained from the China Geological Survey (https://geocloud.cgs.gov.cn/). The river water discharge data from the Hejin stations from 2017 to 2021 were acquired from the National Earth System Science Data Center (http://loess.geodata.cn/index.html).

## 3. Results

### 3.1. Spatiotemporal variation of hydrochemistry

The EC values varied from 1080 to 1218 μS/cm in streamwater, which were lower than those in groundwater (1416–1526 μS/cm) during the four sampling periods (Table 1). The ion composition was similar in streamwater and groundwater, with $Na^+$ and $Ca^{2+}$ being the dominant cations, and $HCO_3^-$ and $SO_4^{2-}$ the dominant anions. Five clusters were identified using the HCA analysis, with mean EC, $Cl^-$ and $Na^+$ values increasing from cluster I to V (Table S1). Hydrochemical variations among these clusters were evident, as depicted by the Piper diagram (Fig. 3b).

The clusters revealed by HCA underscored the hydrochemical connectivity between streamwater and groundwater, particularly evident in the similarities observed in neighboring samples (Fig. 3a). Transitioning from $HCO_3$-Ca types in cluster I—typical of karst water from the upper reaches—to the more evolved Cl-Na type in cluster V signified a clear evolution in water chemistry along the water flow path. Specifically,

**Table 1**
Statistical summary of chemical and isotopic composition of streamwater and groundwater samples in the FRB.

| Date | Type | | T | pH | EC | $Cl^-$ | $SO_4^{2-}$ | $HCO_3^-$ | $NO_3^-$ | $Ca^{2+}$ | $K^+$ | $Mg^{2+}$ | $Na^+$ | δD | $\delta^{18}O$ |
|---|---|---|---|---|---|---|---|---|---|---|---|---|---|---|---|
| May 2019 | SW($n$ = 57) | Ave. | 20.9 | 8.2 | 1221.7 | 94.1 | 220.7 | 243.9 | 20.1 | 96.7 | 8.1 | 33.1 | 88.3 | −66.9 | −9.2 |
| | | S.D. | 3.9 | 0.4 | 785.5 | 128.6 | 288.7 | 92.6 | 27.8 | 75.4 | 9.8 | 28.5 | 106 | 5.7 | 1.2 |
| | GW($n$ = 59) | Ave. | 15.4 | 7.6 | 1420.8 | 87.6 | 234.8 | 470.6 | 29.9 | 114.8 | 2.6 | 51.4 | 117.7 | −72.7 | −10 |
| | | S.D. | 8.3 | 0.4 | 758.9 | 89.4 | 230.9 | 244.2 | 52.2 | 67.4 | 2.8 | 40.3 | 125 | 7.2 | 1.2 |
| September 2019 | SW($n$ = 58) | Ave. | 21 | 8.4 | 1132.4 | 89.7 | 192.8 | 295.3 | 20.9 | 103.2 | 9.6 | 31.2 | 89 | −67.1 | −9.2 |
| | | S.D. | 4.9 | 0.3 | 705.4 | 132 | 244.8 | 101.9 | 25.6 | 63.8 | 10 | 23.9 | 119.3 | 5.9 | 1.3 |
| | GW($n$ = 68) | Ave. | 14 | 7.7 | 1536.2 | 92.3 | 292.3 | 415.5 | 27.3 | 122.7 | 2.5 | 54.2 | 113.1 | −71.7 | −9.9 |
| | | S.D. | 2.7 | 0.2 | 838.5 | 94.7 | 340.2 | 152.8 | 45.6 | 83.9 | 2.3 | 42.1 | 114.7 | 5.5 | 0.9 |
| May 2021 | SW($n$ = 22) | Ave. | 21.5 | 8.1 | 1161.9 | 156.9 | 275.8 | 242.1 | 29.8 | 99 | 8.6 | 45 | 122.7 | −60.8 | −7.9 |
| | | S.D. | 2.4 | 0.4 | 556.6 | 116.7 | 201.9 | 63 | 76.1 | 80.2 | 6.9 | 28.2 | 65.5 | 8.9 | 1.6 |
| | GW($n$ = 8) | Ave. | 17.5 | 7.4 | 1505 | 96.9 | 341 | 368.3 | 45.2 | 64.7 | 3.9 | 40.5 | 91.9 | −72.2 | −10.3 |
| | | S.D. | 3.9 | 0.4 | 974.9 | 84.7 | 375.7 | 86.5 | 75.3 | 48 | 8.7 | 34.2 | 112 | 3.7 | 0.8 |
| August 2021 | SW($n$ = 64) | Ave. | 24.6 | 8.6 | 1139.4 | 129.8 | 247 | 228.8 | 23.3 | 75.9 | 12 | 39.6 | 82.6 | −66.9 | −9 |
| | | S.D. | 2.3 | 0.3 | 440.9 | 96.6 | 145.5 | 68.7 | 17.4 | 35.5 | 8.4 | 14.3 | 44.9 | 4.2 | 0.8 |
| | GW($n$ = 30) | Ave. | 19.2 | 8.5 | 1416 | 113.1 | 363.8 | 430.6 | 33.8 | 89.6 | 7.2 | 51.6 | 116.1 | −72.1 | −9.8 |
| | | S.D. | 3.7 | 0.4 | 971.7 | 120.1 | 543.9 | 175.1 | 50.3 | 84 | 19.8 | 30 | 108 | 6.4 | 0.8 |
| FRB | SW($n$ = 201) | Ave. | 22.2 | 8.4 | 1163.2 | 111.1 | 227.1 | 253.7 | 22.4 | 92.3 | 9.8 | 35.9 | 90.6 | −66.3 | −9 |
| | | S.D. | 4 | 0.4 | 640.1 | 120.5 | 228.3 | 89.5 | 33.4 | 63 | 9.2 | 23.7 | 92.3 | 6.1 | 1.2 |
| | GW($n$ = 165) | Ave. | 15.7 | 7.8 | 1466.9 | 94.8 | 286.7 | 437.1 | 30.5 | 110.2 | 3.5 | 51.9 | 114.4 | −72.2 | −9.9 |
| | | S.D. | 6 | 0.5 | 837.4 | 97.3 | 357 | 195.4 | 50.5 | 77.5 | 9.3 | 38.7 | 116.5 | 6.3 | 1 |

Note: The unit of temperature (T) is °C, the unit of EC is μS/cm, the unites of the main ions are $mg{\cdot}L^{-1}$, the unites of isotope indicators and d-excess are ‰.

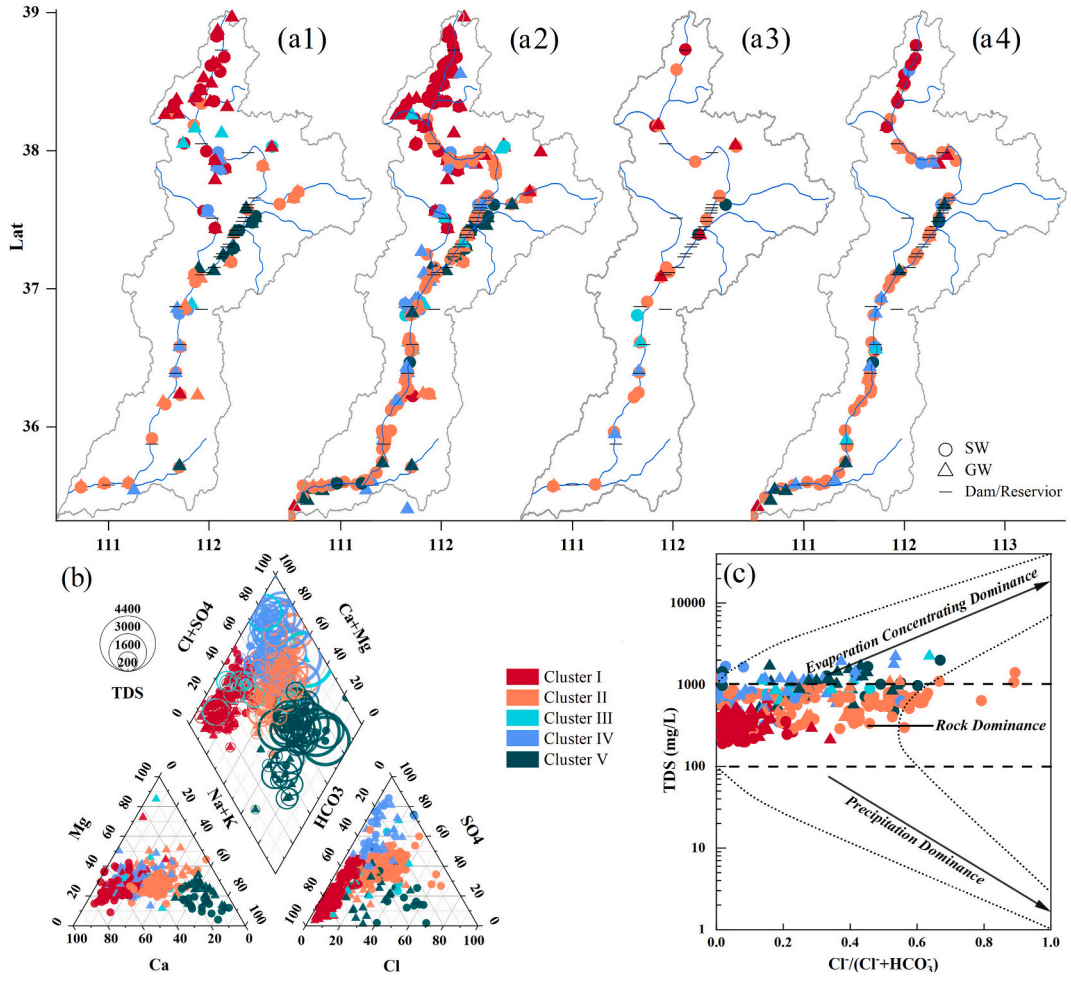


**Fig. 3.** a) Spatial distribution of hydrochemical clustering results in May 2019, September 2019, May 2021 and August 2021, b) Piper diagram, and c) Gibbs diagram. The five clusters (I – V) are represented by different colors.

Cluster II samples, affected by gypsum dissolution, evolved into $SO_4$-$HCO_3$-Ca water types, highlighting the role of natural water-rock interactions. Cluster III, with elevated nitrate levels pointing to anthropogenic influences, was mainly distributed in the upper-middle reaches in 2019 and the lower reaches in 2021. Clusters IV and V, characterized by higher EC values and $SO_4^{2-}$ concentrations (Table S1), were mainly affected by evaporation processes as the samples were closer to the evaporation dominance area (Fig. 3c). Interestingly, river water usually

exhibited more advanced stages of hydrochemical evolution than adjacent groundwater, suggesting a primary directional flow from groundwater to river water.

### 3.2. Spatiotemporal variation of stable isotopes

The average water isotope values of groundwater were −72.7 ‰, −71.7 ‰, −72.2 ‰ and −72.1 ‰ for $\delta^2H$ and −10 ‰, −9.9 ‰, −10.3 ‰, and −9.8 ‰ for $\delta^{18}O$ in May 2019, September 2019, May 2021, and August 2021, respectively. The mean $\delta^2H$ and $\delta^{18}O$ values of streamwater were more enriched than those of groundwater, with corresponding averages of −66.9 ‰, −67.1 ‰, −60.8 ‰ and −66.9 ‰ for $\delta^2H$ and −9.2 ‰, −9.2 ‰, −7.9 ‰, and −9.0 for $\delta^{18}O$, respectively (Table 1). Compared with groundwater $\delta^{18}O$ values, the river water $\delta^{18}O$ values exhibited higher spatiotemporal variability. Temporally, significant seasonal variations in river water $\delta^{18}O$ and d-excess values were observed in 2021, while no significant intra-annual variations were observed in 2019 (Fig. 4). Spatially, enriched isotopes and lower d-excess values were observed in the middle reaches in groundwater, especially during wet seasons, suggesting the effect of streamwater infiltration in these sections (Fig. 4).

The water sampling sites were close and mainly located at the bottom right of the LMWL (Fig. 5a), indicating that the streamwater and groundwater were primarily recharged by precipitation but subjected to evaporation. Temporally, the lower slopes and intercepts of the evaporation line (EL) confirmed that the water evaporation was stronger in 2019 than in 2021 due to the influence of drought (Table S3). Groundwater, overall, had experienced less evaporation compared with streamwater, as indicated by higher d-excess values (Fig. 5b). Spatially, the d-excess values of water samples exhibited lower values in the middle reaches than in other reaches, indicating stronger evaporation in this river section possibly due to the presence of dams and reservoirs (Fig. 4). Furthermore, several groundwater samples had exhibited lower d-excess values than streamwater samples, suggesting the effect of streamwater infiltration and continuous evaporation due to elevated water levels.

### 3.3. Identifying and quantifying SGI

Most streamwater samples overlapped with groundwater but exhibited enriched isotope values (Fig. 5). This pattern aligned with the source-sink theory, where the sink water usually located on the right side of source water (Kendall and Doctor, 2003), suggesting the predominant SGI pattern of groundwater discharging into streamwater. Theoretically, river water isotopes should exhibit an increasing trend towards the downstream as a result of evaporation if no external water sources input. However, the stability or decline in streamwater $\delta^{18}O$ values from upstream to downstream (Fig. 6) indicated an obvious SGI relationship of groundwater discharging into streamwater. In contrast, a distinct enrichment in $\delta^{18}O$ in groundwater, accompanied by higher $Cl^-$ concentrations, was observed primarily in the upper and middle reaches in 2019 and the lower reaches in August 2021, signifying the substantial influence of river water infiltration.

Specifically, during May 2019, higher $\delta^{18}O$ and $Cl^-$ values, along with lower d-excess values were observed in groundwater and tributaries within the 100–300 km segments (Fig. 6), predominantly on the left bank, suggesting the infiltration of streamwater into the left bank groundwater within this specific segment. The correlation between increasing groundwater $Cl^-$ concentrations and closer proximity to the riverbank underscored a distance-dependent influence of streamwater on groundwater. During September 2019, a notable increase in streamwater $\delta^{18}O$ values along the river channel in the upper and middle reaches, accompanied by increasing $\delta^{18}O$, $Cl^-$ values and decreasing d-excess values in groundwater, suggested streamwater

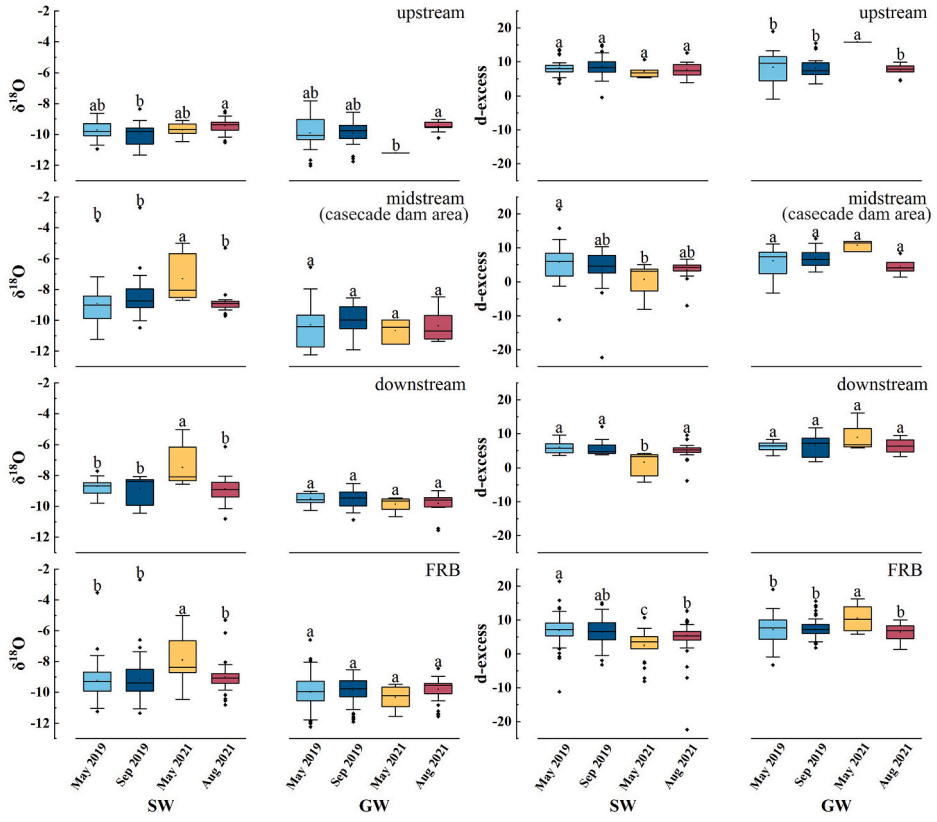


**Fig. 4.** Spatiotemporal variation of $\delta^{18}O$ (left panel) and d-excess (right panel) in streamwater and groundwater from the upper to lower reaches of the FRB. The distinct lowercase letters reveal significant differences among different reaches/years at a significance level of $p = 0.05$.

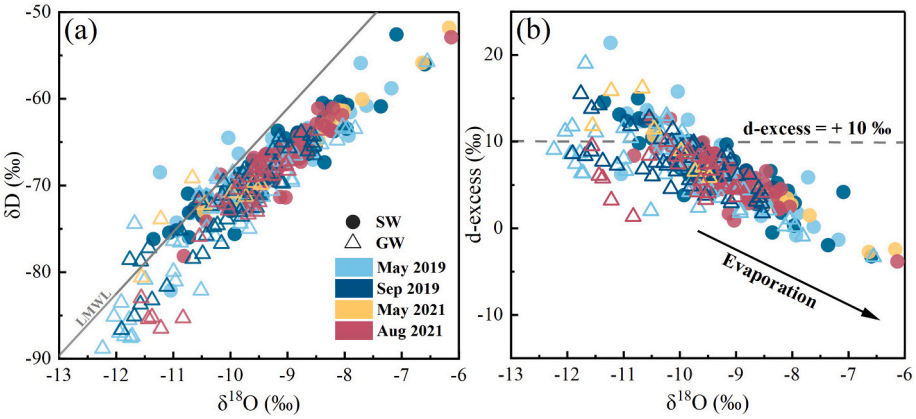


**Fig. 5.** Comparison of $\delta^2H$ and $\delta^{18}O$ of streamwater (SW) and groundwater (GW) samples (a) and $\delta^{18}O$ versus d-excess (b). The Local Meteoric Water Line (LMWL: $\delta^2H = 7.13\ \delta^{18}O + 3.06$) is referred from previous studies in the FRB (Liu et al., 2021).

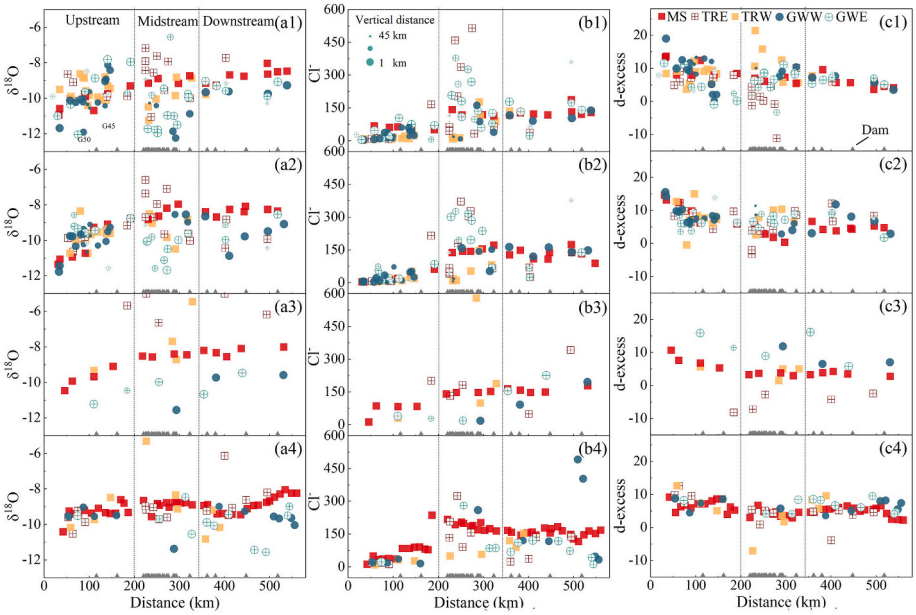


**Fig. 6.** Spatial patterns of $\delta^{18}O$ (a1-a4), $Cl^-$ (b1-b4) and d-excess (c1-c4) in streamwater and groundwater in May 2019, September 2019, May 2021 and August 2021. The size of groundwater sample points depends on the vertical distance between the sample points and the river. MS, TRE, TRW, GWE and GWW represent mainstream, tributaries flowing in from the east bank, tributaries flowing in from the west bank, groundwater on the east bank and west bank, respectively.

recharging groundwater in these segments. In contrast, lower groundwater $\delta^{18}O$ values and higher d-excess values compared to streamwater in May and August 2021 indicated that the SGI was dominated by groundwater discharging to streamwater. However, an increasing trend in streamwater $\delta^{18}O$, coupled with higher $Cl^-$ concentrations in specific groundwater sampling points, was observed in the lower reaches in August 2021, indicating localized streamwater infiltration at these sites.

Point-by-point tracer comparison between adjacent streamwater and groundwater enabled the identification of source-sink relationships across segments and the quantification of source contributions (Fig. S2). Despite the differences in the number and location of sampling sites for different sampling periods, the dominant SGI directions in various reaches could be inferred from the proportion of exchange types. Approximately 60 % of the sampling sites showed an SGI relationship of groundwater discharging to streamwater, with discharge ratios of 12 %–54 % (averaged at each sampling site) (Table S4 and Fig. 7). Temporally, the discharge ratios were higher in 2019, with mean values of 31 % in May 2019 and 30 % in September 2019, compared to 2021 (24 % in May 2021 and 17 % in Aug 2021) across the whole watershed. Spatially, the groundwater discharge ratios decreased from the upper to the lower reaches, with the lowest groundwater discharge ratios observed in the cascade dam area. Conversely, the sample groups with streamwater recharging groundwater exhibited higher proportions in May 2019 (62 %) and September 2019 (54 %) compared to August 2021 (36 %) and May 2021 (29 %) (Fig. 7 and Table S4). Specifically, this exchange pattern was mainly observed in the upper and middle reaches in 2019, with an average contribution ranging from 29 % to 78 % (Table S4 and Fig. 7). These quantitative results align with the above qualitative analysis, further confirmed the reliability of multi-tracer analysis.

## 4. Discussions

### 4.1. What is the impact of precipitation anomalies on SGI?

Interannual variations in water chemical types, isotope values, and SGI were found to be more pronounced than the seasonal variations in the FRB (Fig. 4, Fig. 6, and Fig. 7). For instance, the proportion of streamwater clustering showed significant differences between 2019

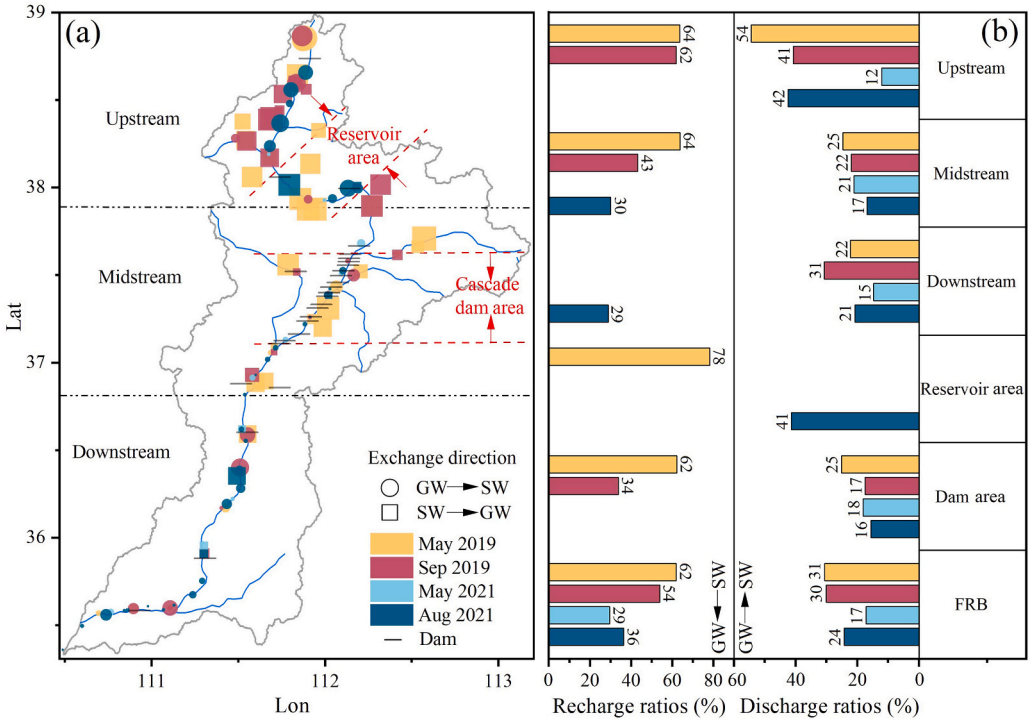


**Fig. 7.** a) Spatiotemporal distribution of SGI exchange ratios in the sampling periods, b) bar charts of streamwater recharge ratios and groundwater discharge ratios in various reaches. To reduce random errors, the number of sample groups <2 in each reach is not counted.

and 2021, exceeding the variations observed within seasons. And more evolved water types and TDS values were observed in 2019 compared to 2021 (Fig. S3). At groundwater sampling sites, Cluster I maintained nearly consistent proportions in May 2019 (39 %) and September 2019 (38 %) (Table S2). These variations can be linked to the stark contrast in annual precipitation—marked by extreme drought in 2019 and high humidity in 2021—elucidating the spatiotemporal impact of precipitation on SGI.

Before 2019 sampling, Northern China, including the FRB, faced a prolonged drought that significantly altered the hydrological cycle (Guo et al., 2023). Drought conditions enhanced sub-cloud secondary evaporation, leading to the enrichment of isotopes in precipitation (Cai et al., 2017), which in turn enriched streamwater isotopes through increased surface evaporation (Wu et al., 2022). This phenomenon was evident in 2019, as streamwater evaporation line slopes and intercepts were lower than in 2021 (Table S3), indicating strong evaporation and isotope fractionation. Consequently, the river's water level lowered and flow diminished, particularly in the lower reaches characterized by numerous tributaries and fewer dams compared to the upper and middle reaches. Specifically, the drought in 2019 decreased the annual runoff to just 28 % of that in 2021. These shifts increased the proportion of equivalent groundwater discharge in river water, with groundwater discharge ratios rising by over 46 % in 2019 (22 % and 31 % in the dry and wet seasons, respectively) compared to 2021 (15 % and 21 %) during both seasons. Long-term monitoring further revealed that consecutive droughts had diminished the response of river flow to summer precipitation events from 2017 to 2019 (Fig. S1), underscoring groundwater's increased contribution to baseflow during drought periods.

In contrast, the abundant precipitation in August 2021 significantly increased both river flow and groundwater levels, complicating the SGI dynamics. Specifically, the river flow surged by 54–967 $m^3/s$, with groundwater levels rising by up to 2 m compared to 2019 (Fig. S1). The extreme rainfall event in 2021 increased river flow in the lower reaches by 7.4 times compared to 2019, surpassing the relative increases in precipitation (2.2 times) and groundwater levels (1.1 times). This transient flood significantly recharged groundwater, since rapid responses of groundwater levels to flood and precipitation were observed during flood periods (Fig. S1) (Doppler et al., 2007; Geris et al., 2022), which can be further confirmed by the isotopic evidence (a closer alignment of sampling sites to the LMWL) (Fig. 5). Such dynamics suggest a pronounced impact of precipitation on water cycle dynamics under flood conditions (Scanlon et al., 2003). Moreover, the precipitation percolation rates exhibited spatial variability, with areas far from the river channel, particularly karst mountain regions, showing higher percolation rates due to macropores (Peng and Wang, 2012); while the percolation rates were obviously reduced in alluvial plains close to the riverbank, which were capped by a fine loess layer (Ming-bin et al., 2001; Peng and Wang, 2012). Thus, more depleted groundwater isotopes were observed in areas far from rivers (Fig. 6). This spatial disparity in groundwater recharge mechanisms fostered stronger lateral groundwater flows in 2021, particularly affecting the SGI dynamics by enhancing groundwater discharge to streamwater in the upper and middle reaches of the FRB (Fig. 7).

The impact of precipitation anomalies on SGI dynamics has been extensively studied globally, and the specific mechanisms vary with research areas. For instance, severe droughts in North America have led to declining alluvial groundwater tables and reversed flow directions between streamwater and groundwater across extensive river reaches (Scanlon et al., 2003). A continental-scale study, involving over 4.2 million wells and their adjacent stream segments, indicated that losing rivers are more prevalent in areas with drier climates, flatter landscapes, and extensive groundwater pumping (Jasechko et al., 2021). Meteorological drought reduces groundwater recharge and increases regional water extraction, impacting groundwater levels more significantly than river flows. Global estimates of groundwater depletion using both flux-based and volume-based methods identified that the depletion is most pronounced in North America and Asia (China, India) but very noticeable in Australia where extraction is governed by regulations such as cease-to-pump rules (Reinfelds et al., 2004; Taylor et al., 2012). As such, groundwater level dynamics are more sensitive to drought than river flow, finally becoming the dominant factors controlling SGI dynamics at the watershed scale.

### 4.2. How do dams influence the spatiotemporal variations in SGI?

Groundwater traditionally serves as the primary and even the sole source of river flow, especially during dry seasons (Kelly et al., 2019). However, our findings revealed that in areas impounded by dams, most streamwater recharged groundwater during both dry and wet sampling periods, highlighting the profound impact of dams/reservoirs in altering traditional SGI dynamics. Notably, isotopic variation patterns shifted distinctly between the periods before (2019) and after the dam opening (2021). In 2019, streamwater isotopes showed a slight enrichment trend with distance (Fig. 6). However, the 2021 flood event introduced isotopically depleted runoff that mixed rapidly within the river channel, causing the homogenization of river water with lower fluctuations of $\delta^{18}O$ and d-excess in damming reaches (Fig. 6) (Wu et al., 2022). Ultimately, the contribution of streamwater to groundwater reached as high as 78 % in reservoir areas and 64 % in dam areas, far surpassing regions unaffected or minimally influenced by dams (0–29 %) (Fig. 7). Moreover, groundwater in dam-operated areas exhibited more elevated water types (Cluster III-V) compared to areas without dams (Fig. 3a), further suggesting an increase in anthropogenic inputs, soil leaching and water-rock interaction due to streamwater infiltration (Xia et al., 2024).

However, the impact of streamwater infiltration occurred only within a limited distance. Groundwater samples close to the rivers usually exhibited enriched isotopes and higher $Cl^-$ concentrations (Fig. 6). This was further confirmed by the significant negative correlation relationship ($p < 0.05$) between streamwater recharge ratios and lateral distance. The streamwater infiltration ratios decreased rapidly after groundwater samples were beyond 1 km from the riverbank, with the maximum affect distance of about 3 km (Fig. S4). This confirmed the localized influence of rivers on groundwater recharge, aligning with a prior research that indicated a diminishing streamwater contribution with increasing distance from the river (Hong et al., 2022).

Dams and reservoirs facilitate not only a one-way water flux exchange vertically and laterally but also create a hydrological "discontinuum", affecting longitudinal hydraulic connectivity (Boulton et al., 2017). During the dam impounding period, the d-excess value of upstream river water rapidly decreased as it approached the dam, indicating that the hydraulic interception of the dam increased the hydraulic residence time and promoted evaporation (Jiang et al., 2021; Wu et al., 2022). Concurrently, groundwater d-excess trends mirrored those of streamwater in front of the dam, indicating significant river infiltration into groundwater. The shift from river water infiltration to groundwater discharges was evident, because streamwater d-excess values decreased upstream of the dam but increased downstream. This highlights a reversal in dominant SGI dynamics when water moved through the dam. This phenomenon was quantitatively supported by the fact that groundwater discharge ratios at sites downstream of the dam (60 %) were threefold those upstream (Fig. 8c). The hydraulic interception of the dam significantly increased groundwater levels upstream and reduced downstream river water flow (Wang et al., 2018). Such dynamics established steeper hydraulic gradients between underground reservoirs and the riverbed, facilitating groundwater discharge downstream of the dams/reservoirs. However, the 2021 opening of the dam marked a significant change: both river water and groundwater d-excess values increased downstream, and $\delta^{18}O$ values in groundwater became more depleted than in river water, suggesting that groundwater stably replenished river water in this scenario. The stable groundwater discharge ratios along the longitudinal direction further demonstrated the diminished regulatory effect of dams on SGI (Fig. 8).

Furthermore, the impact of cascade dams on water chemistry, isotopic composition, and d-excess presents a more complex pattern compared to the influence of a single dam. A significant negative correlation ($p < 0.05$) was observed between groundwater discharge ratios and dam/reservoir density. The cascade dams altered SGI directions by

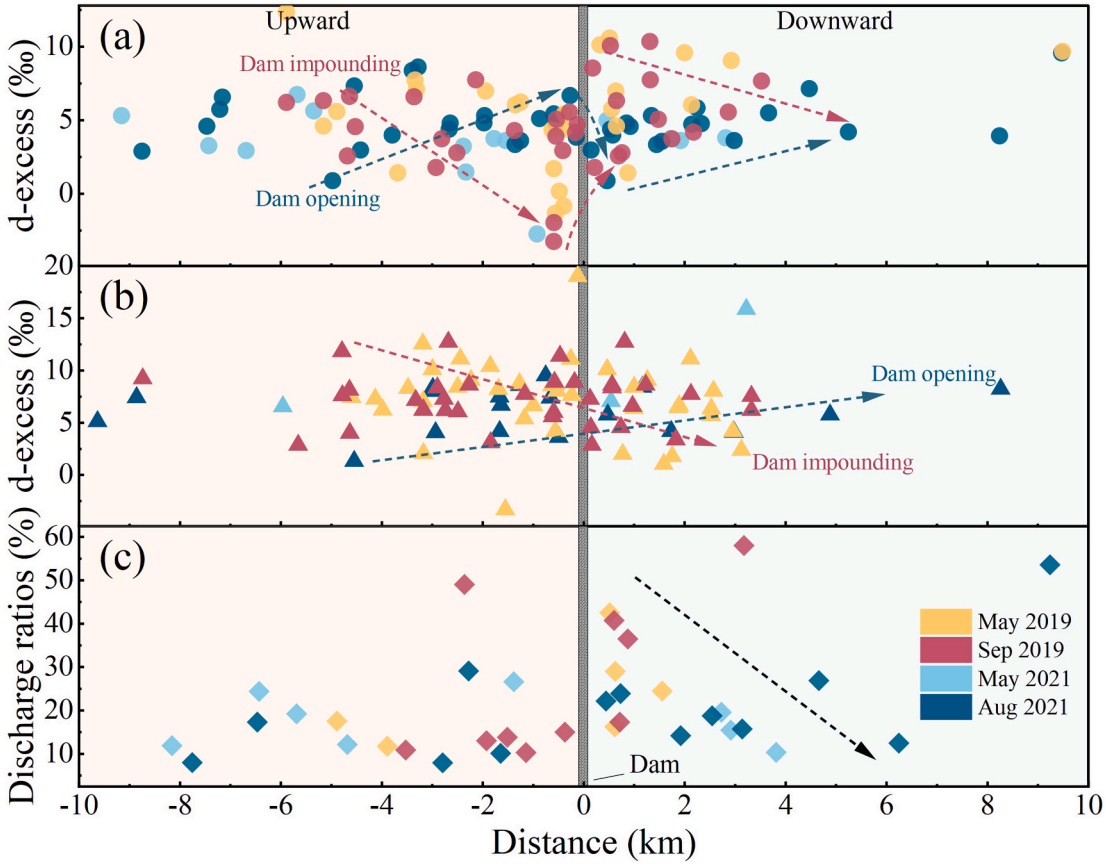


**Fig. 8.** The d-excess values in streamwater (a) and groundwater (b) and groundwater discharge ratios at different distances upstream and downstream of the dams.

regulating water levels and increasing water evaporation, resulting in cumulative effects on the variation of water isotopes that were much greater than the impact of a single dam (Jiang et al., 2021). This finding aligned with studies on dammed rivers globally, such as the Yangtze River (Zhou and Zhou, 2023), Meigong River (Pokhrel et al., 2018), Dagu River (Jiang et al., 2021), and the Amazon basin (Athayde et al., 2019), where cascade dams have significantly influenced SGI variations.

Overall, the SGI pattern can be profoundly altered by dam and reservoir regulations across different dimensions—laterally, vertically, and longitudinally—during impoundment and release periods. These changes, manifested through adjustments in water level, evaporation rates, and river morphology, underscored the substantial influence of dams and reservoirs on disrupting natural water flux patterns.

### 4.3. What are the combined effects of damming and extreme climate events on SGI?

The results highlight the critical roles of extreme climate events and river damming in shaping the SGI dynamics at the watershed scale. Notably, these two impact factors are also interrelated. Climate variability can influence dam regulation regimes, while damming activities may exacerbate drought conditions by increasing evaporation and water extraction or mitigate flood impacts by intercepting peak flows and regulating river discharge (Best, 2019; Jiang et al., 2021). The contrasting precipitation patterns observed in 2019 and 2021 have necessitated heightened human intervention in the FRB's river system, significantly altering the hydrological cycle and SGI dynamics by impacting water evaporation, recharge, and hydraulic residence time.

However, the dominance of the effects of extreme climate events and dams varies across scenarios. Extreme climate events broadly impact water cycle dynamics, whereas the impacts of dams, though more localized, can dramatically reshape hydrology within affected areas. For example, dam impoundment has moderated the seasonal effect of precipitation, facilitating streamwater infiltration during both dry and flood seasons in 2019 (Fig. 7). The manipulation of hydrology by reservoirs and check dams has distinctly altered SGI patterns, particularly in critical dam regions, across both dry and wet periods. Such anthropogenic modifications have significantly overshadowed the effects of natural climatic extremes on water resources and the water cycle, offering a buffer against the harsh impacts of these events.

Building on this analysis, our conceptual model elucidates the hydrological cycle and SGI in the FRB under the combined influences of precipitation anomalies and damming (Fig. 2). During droughts, dams intercept hydraulic flows, raising upstream water levels and reducing downstream flow, while also extending the hydraulic residence time and promoting evaporation of streamwater. These alterations lead to streamwater infiltration into groundwater upstream of the dam, subsequently enhancing groundwater discharge to streamwater downstream. Conversely, during flood seasons, rainstorm replenishes groundwater rapidly through large pores in mountainous areas, raising groundwater levels. With dams open for flood prevention, river water levels both in front of and behind the dam tend to normalize, facilitating stable groundwater replenishment to river flows.

### 4.4. Implications

This study underscored the complex interplay between human interventions and natural climatic variations, emphasizing the need for adaptive management strategies that consider the intricate dynamics of SGI under changing climatic conditions. Groundwater levels emerge as critical to SGI dynamics. While dams and reservoirs can modify the natural patterns of SGI at reach scales, their influence on groundwater is primarily localized near riverbanks (within 3 km in this study), limited by topographical and storage capacity disparities between river and groundwater systems. Consequently, dam-based groundwater replenishment is only marginally effective. Conversely, significant rainfall events can swiftly augment watershed-wide groundwater levels (Fig. S1), highlighting the necessity of incorporating adaptive anthropogenic strategies within water management frameworks. Strategies like Managed Aquifer Recharge (MAR) and Aquifer Storage and Recovery (ASR) are pivotal in augmenting groundwater during climatic extremes, by storing excess water for future use (Dillon et al., 2018; Shandilya et al., 2022). Furthermore, the global groundwater decline, tied to over-extraction (Reinfelds et al., 2004; Taylor et al., 2012), accentuates the imperative of embracing water-saving innovations and practices in agriculture, industry, and domestic spheres. Promoting efficient irrigation and wastewater reuse is vital for curbing groundwater depletion and aiding in the restoration of ecological baseflows.

However, challenges remain in quantifying these impacts across different dimensions—dams in the spatial dimension and precipitation in the temporal dimension. Therefore, there is an urgent need to enhance sampling frequency within large basins for future research. Utilizing long-term runoff and water level data can contribute to understanding the effects of precipitation anomalies and dam operations on SGI dynamics (Quang et al., 2023). Because of the impact of COVID-19, this study encountered challenges in maintaining sampling point consistency across different periods, as seen with fewer samples for May 2021. Although this discrepancy does not hinder SGI identification during these periods, it remains crucial to maintain consistency in sampling points to exclude the potential impact on data quality and interpretation in future studies.

## 5. Conclusions

The combined effects of precipitation anomalies and damming on SGI were investigated using tracer-based methods in a highly regulated river during four sampling campaigns across extreme drought and flood years. This study revealed that the flow path of groundwater discharging into streamwater predominantly governed the SGI across the entire watershed. Conversely, streamwater recharging groundwater was primarily observed in regions with impounded dams/reservoirs, especially the drought year, highlighting the significant control exerted by both precipitation and damming over SGI patterns. Specifically, the drought of 2019 led to increased river water evaporation and a reduction in river flow, indirectly enhancing the contribution of groundwater to river water. In contrast, the floods of 2021 elevated groundwater levels, thereby enhancing the discharge of groundwater into streamwater. Damming activities were found to significantly raise river water levels, facilitating one-way water infiltration, although their impact was confined to a horizontal extent of up to 3 km from the river channel. The combined effects of precipitation anomalies and damming introduces significant variability in hydrological cycle and SGI regimes at the watershed scale. These findings underline the critical need for adaptive water resource management strategies that effectively integrate the multifaceted impacts of dam regulation and precipitation anomalies within future frameworks.

## CRediT authorship contribution statement

**Yun Xia:** Conceptualization, Methodology, Software, Formal analysis, Visualization, Writing – original draft. **Jun Xiao:** Funding acquisition, Validation, Data curation, Writing – review & editing. **Martine van der Ploeg:** Writing – review & editing, Supervision. **Wanzhou Wang:** Resources, Formal analysis. **Zhi Li:** Writing – review & editing, Supervision, Resources, Project administration, Funding acquisition, Conceptualization.

## Declaration of competing interest

The authors declare that they have no known competing financial interests or personal relationships that could have appeared to influence the work reported in this paper.

## Data availability

Data will be made available on request.

## Acknowledgments

This study is jointly funded by the National Natural Science Foundation of China (42071043), Chinese Universities Scientific Funding (2452023276), the Strategic Priority Research Program of Chinese Academy of Sciences (XDB40020500), and Western Light-Key Laboratory Cooperative Research Cross-Team Project of Chinese Academy of Sciences (xbzg-zdsys-202309).

## Appendix A. Supplementary data

Supplementary data to this article can be found online at https://doi.org/10.1016/j.scitotenv.2024.172704.

## References

Athayde, S., Duarte, C.G., Gallardo, A.L.C.F., et al., 2019. Improving policies and instruments to address cumulative impacts of small hydropower in the Amazon. Energy Policy 132, 265–271.
Best, J., 2019. Anthropogenic stresses on the world's big rivers. Nat. Geosci. 12, 7–21.
Boulton, A.J., Rolls, R.J., Jaeger, K.L., Datry, T., 2017. Hydrological connectivity in intermittent rivers and ephemeral streams. In: Intermittent Rivers and Ephemeral Streams, pp. 79–108.
Cai, Z., Tian, L., Bowen, G.J., 2017. ENSO variability reflected in precipitation oxygen isotopes across the Asian Summer Monsoon region. Earth Planet. Sci. Lett. 475, 25–33.
Coutino, A., Stastna, M., Reinhardt, E.G., 2020. Interaction of mangrove surface coverage and groundwater inputs on the temperature and water level near Tulum, Quintana Roo, Mexico: observations and modelling. J. Hydrol. 583.
Dey, S., Saksena, S., Winter, D., Merwade, V., McMillan, S., 2022. Incorporating network scale river bathymetry to improve characterization of fluvial processes in flood modeling. Water Resour. Res. 58.
Dillon, P., Stuyfzand, P., Grischek, T., et al., 2018. Sixty years of global progress in managed aquifer recharge. Hydrgeol. J. 27, 1–30.
Doppler, T., Franssen, H.-J.H., Kaiser, H.-P., Kuhlman, U., Stauffer, F., 2007. Field evidence of a dynamic leakage coefficient for modelling river–aquifer interactions. J. Hydrol. 347, 177–187.
Dudley-Southern, M., Binley, A., 2015. Temporal responses of groundwater-surface water exchange to successive storm events. Water Resour. Res. 51, 1112–1126.
Francis, B.A., Francis, L.K., Cardenas, M.B., 2010. Water table dynamics and groundwater-surface water interaction during filling and draining of a large fluvial island due to dam-induced river stage fluctuations. Water Resour. Res. 46.
Frei, R., Frei, K.M., Kristiansen, S.M., Jessen, S., Schullehner, J., Hansen, B., 2020. The link between surface water and groundwater-based drinking water – strontium isotope spatial distribution patterns and their relationships to Danish sediments. Appl. Geochem. 121.
Fuchs, E.H., King, J.P., Carroll, K.C., 2019. Quantifying disconnection of groundwater from managed-ephemeral surface water during drought and conjunctive agricultural use. Water Resour. Res. 55, 5871–5890.
Geris, J., Comte, J.-C., Franchi, F., et al., 2022. Surface water-groundwater interactions and local land use control water quality impacts of extreme rainfall and flooding in a vulnerable semi-arid region of Sub-Saharan Africa. J. Hydrol. 609.
Gibbs, R.J., 1970. Mechanisms controlling world water. Chemistry 170, 1088–1090.
Grill, G., Lehner, B., Thieme, M., et al., 2019. Mapping the world's free-flowing rivers. Nature 569, 215–221.
Guevara-Ochoa, C., Medina-Sierra, A., Vives, L., 2020. Spatio-temporal effect of climate change on water balance and interactions between groundwater and surface water in plains. Sci. Total Environ. 722, 137886.
Guggenmos, M.R., Daughney, C.J., Jackson, B.M., Morgenstern, U., 2011. Regional-scale identification of groundwater-surface water interaction using hydrochemistry and multivariate statistical methods, Wairarapa Valley, New Zealand. Hydrol. Earth Syst. Sci. 15, 3383–3398.
Guo, C., Shi, J., Zhang, Z., Zhang, F., 2019. Using tritium and radiocarbon to determine groundwater age and delineate the flow regime in the Taiyuan Basin, China. Arab. J. Geosci. 12.
Guo, Y., Huang, G., Guo, Q., et al., 2023. Increase in root density induced by coronatine improves maize drought resistance in North China. Crop J. 11, 278–290.
Herrera, C., Urrutia, J., Gamboa, C., et al., 2023. Evaluation of the impact of the intensive exploitation of groundwater and the mega-drought based on the hydrochemical and isotopic composition of the waters of the Chacabuco-Polpaico basin in central Chile. Sci. Total Environ. 895, 165055.
Hong, Z., Ding, S., Zhao, Q., et al., 2022. Relative contribution of multi-source water recharge to riparian wetlands along the lower Yellow River. J. Environ. Manage. 321, 115804.
Hu, Y., Fan, H., Zhao, M., et al., 2023. Differences in watershed evaporation indicated by hydrogen and oxygen single and dual isotopes: evidence from controlled simulation tests under different land uses. J. Hydrol. 617.
IPCC, 2021. Climate Change 2021: The Physical Science Basis. Contribution of Working Group I to the Sixth Assessment Report of the Intergovernmental Panel on Climate Change. Cambridge University Press, p. 2391.
Jasechko, S., Seybold, H., Perrone, D., Fan, Y., Kirchner, J.W., 2021. Widespread potential loss of streamflow into underlying aquifers across the USA. Nature 591, 391–395.
Jiang, D., Li, Z., Luo, Y., Xia, Y., 2021. River damming and drought affect water cycle dynamics in an ephemeral river based on stable isotopes: the Dagu River of North China. Sci. Total Environ. 758, 143682.
Jiang, D., Li, Z., Xia, Y., Li, Y., Luo, Y., 2022. Combined effects of damming and drought on nitrogen dynamics in an ephemeral river of North China. J. Clean. Prod. 373, 133940.
Jutebring Sterte, E., Johansson, E., Sjöberg, Y., Huseby Karlsen, R., Laudon, H., 2018. Groundwater-surface water interactions across scales in a boreal landscape investigated using a numerical modelling approach. J. Hydrol. 560, 184–201.
Kelly, L., Kalin, R.M., Bertram, D., Kanjaye, M., Nkhata, M., Sibande, H., 2019. Quantification of temporal variations in base flow index using sporadic river data: application to the Bua Catchment, Malawi. Water 11.
Kendall, C., Doctor, D.H., 2003. 5.11 - stable isotope applications in hydrologic studies. In: Holland, H.D., Turekian, K.K. (Eds.), Treatise on Geochemistry. Pergamon, Oxford, pp. 319–364.
King, A.C., Raiber, M., Cendón, D.I., Cox, M.E., Hollins, S.E., 2015. Identifying flood recharge and inter-aquifer connectivity using multiple isotopes in subtropical Australia. Hydrol. Earth Syst. Sci. 19, 2315–2335.
Kondolf, G.M., Rubin, Z.K., Minear, J.T., 2014. Dams on the Mekong: cumulative sediment starvation. Water Resour. Res. 50, 5158–5169.
Latrubesse, E.M., Arima, E.Y., Dunne, T., et al., 2017. Damming the rivers of the Amazon basin. Nature 546, 363–369.
Li, Z., Lin, X., Coles, A.E., Chen, X., 2017. Catchment-scale surface water-groundwater connectivity on China's Loess Plateau. Catena 152, 268–276.
Li, B., Yang, L., Song, X., Diamantopoulos, E., 2023. Identifying surface water and groundwater interactions using multiple experimental methods in the riparian zone of the polluted and disturbed Shaying River, China. Sci. Total Environ. 875, 162616.
Liu, X., Xiang, W., Si, B., 2021. Hydrochemical and isotopic characteristics in the shallow groundwater of the Fenhe River basin and indicative significance. Environ. Sci. 42, 1739–1749.
Malzone, J.M., Lowry, C.S., Ward, A.S., 2016. Response of the hyporheic zone to transient groundwater fluctuations on the annual and storm event time scales. Water Resour. Res. 52, 5301–5321.
Martínez-Santos, P., Martínez-Alfaro, P.E., Sanz, E., Galindo, A., 2010. Daily scale modelling of aquifer–river connectivity in the urban alluvial aquifer in Langreo, Spain. Hydrogeol. J. 18, 1525–1537.
Miao, C., Zheng, H., Jiao, J., Feng, X., Duan, Q., Mpofu, E., 2020. The changing relationship between rainfall and surface runoff on the Loess Plateau, China. J. Geophys. Res. Atmos. 125.
Ming-bin, H., Fu-hong, H., Xin-min, Y., Yu-shan, L., 2001. Effect of apple production base on regional water cycle in Weibei upland of the Loess Plateau. J. Geogr. Sci. 11, 239–243.
Modie, L.T., Kenabatho, P.K., Stephens, M., Mosekiemang, T., 2022. Investigating groundwater and surface water interactions using stable isotopes and hydrochemistry in the Notwane River Catchment, South East Botswana. J. Hydrol. Reg. Stud. 40.
Parnell, A.C., Inger, R., Bearhop, S., Jackson, A.L., 2010. Source partitioning using stable isotopes: coping with too much variation. PloS One 5, e9672.
Partington, D., Knowling, M.J., Simmons, C.T., et al., 2020. Worth of hydraulic and water chemistry observation data in terms of the reliability of surface water-groundwater exchange flux predictions under varied flow conditions. J. Hydrol. 590.
Peng, T., Wang, S.-j., 2012. Effects of land use, land cover and rainfall regimes on the surface runoff and soil loss on karst slopes in southwest China. Catena 90, 53–62.
Pokhrel, Y., Burbano, M., Roush, J., Kang, H., Sridhar, V., Hyndman, D., 2018. A review of the integrated effects of changing climate, land use, and dams on Mekong River hydrology. Water 10.
Qu, S., Duan, L., Mao, H., et al., 2023. Hydrochemical and isotopic fingerprints of groundwater origin and evolution in the Urangulan River basin, China's Loess Plateau. Sci. Total Environ. 866.
Quang, N.H., Viet, T.Q., Thang, H.N., Hieu, N.T.D., 2023. Long-term water level dynamics in the Red River basin in response to anthropogenic activities and climate change. Sci. Total Environ. 912, 168985.
Reinfelds, I., Haeusler, T., Brooks, A.J., Williams, S., 2004. Refinement of the wetted perimeter breakpoint method for setting cease-to-pump limits or minimum environmental flows. River Res. Appl. 20, 671–685.
Scanlon, B.R., Mace, R.E., Barrett, M.E., Smith, B., 2003. Can we simulate regional groundwater flow in a karst system using equivalent porous media models? Case study, Barton Springs Edwards aquifer, USA. J. Hydrol. 276, 137–158.
Shandilya, R.N., Bresciani, E., Runkel, A.C., Jennings, C.E., Lee, S., Kang, P.K., 2022. Aquifer-scale mapping of injection capacity for potential aquifer storage and recovery sites: methodology development and case studies in Minnesota, USA. J. Hydrol. Reg. Stud. 40.
Shen, H., Li, J., Han, S., et al., 2022. Water resources utilization and eco-environment problem of Fenhe River, branch of Yellow river. Geol. China 49, 1127–1138.
Song, J., Cheng, D., Zhang, J., et al., 2019. Estimating spatial pattern of hyporheic water exchange in slack water pool. J. Geogr. Sci. 29, 377–388.

Taylor, R.G., Scanlon, B., Döll, P., et al., 2012. Ground water and climate change. Nat. Clim. Chang. 3, 322–329.
Unland, N.P., Cartwright, I., Andersen, M.S., et al., 2013. Investigating the spatio-temporal variability in groundwater and surface water interactions: a multi-technique approach. Hydrol. Earth Syst. Sci. 17, 3437–3453.
Wang, D., Jian, S., Wu, Z., Zhang, Z., Hu, C., 2018. Quantitative analysis on sensitive factors of runoff change in Fenhe watershed based on integration approach. Proc. Int. Assoc. Hydrol. Sci. 379, 371–380.
Wang, Y., Lei, X., Wen, X., et al., 2019. Effects of damming and climatic change on the eco-hydrological system: a case study in the Yalong River, southwest China. Ecol. Indic. 105, 663–674.
Wang, Z., Yang, Y., Chen, G., Wu, J., Wu, J., 2021. Variation of lake-river-aquifer interactions induced by human activity and climatic condition in Poyang Lake Basin, China. J. Hydrol. 595.
Wang, W., Li, Z., Su, H., Xiao, J., Han, F., Li, Z., 2022. Spatial and seasonal variability, control factors and health risk of fluoride in natural water in the Loess Plateau of China. J. Hazard. Mater. 434, 128897.
Wang, W., Sun, J., Xia, Y., Li, Z., 2023a. Identifying hydraulic connectivity among the vadose zone, unconfined and confined aquifers in the thick loess deposits using multiple tracers. J. Hydrol. 626.
Wang, X., Jia, S., Xu, Y.J., Liu, Z., Mao, B., 2023b. Dual stable isotopes to rethink the watershed-scale spatiotemporal interaction between surface water and groundwater. J. Environ. Manage. 351, 119728.
Wu, H., Li, J., Song, F., et al., 2018. Spatial and temporal patterns of stable water isotopes along the Yangtze River during two drought years. Hydrol. Process. 32, 4–16.
Wu, H., Song, F., Li, J., Zhou, Y., Zhang, J., Fu, C., 2022. Surface water isoscapes (δ18O and δ2H) reveal dual effects of damming and drought on the Yangtze River water cycles. J. Hydrol. 610.
Xia, Y., Xiao, J., Wang, W., Li, Z., 2024. Nitrate dynamics in the streamwater-groundwater interaction system: sources, fate, and controls. Sci. Total Environ. 918, 170574.
Xiao, J., Wang, L., Chai, N., Liu, T., Jin, Z., Rinklebe, J., 2021. Groundwater hydrochemistry, source identification and pollution assessment in intensive industrial areas, eastern Chinese loess plateau. Environ. Pollut. 278, 116930.
Xie, C., Liu, H., Li, X., et al., 2024. Spatial characteristics of hydrochemistry and stable isotopes in river and groundwater, and runoff components in the Shule River Basin, Northeastern of Tibet Plateau. J. Environ. Manage. 349, 119512.
Yan, X., Sun, J., Huang, Y., Xia, Y., Wang, Z., Li, Z., 2023. Detecting and attributing the changes in baseflow in China's Loess Plateau. J. Hydrol. 617.
Yang, N., Zhou, P., Wang, G., et al., 2021. Hydrochemical and isotopic interpretation of interactions between surface water and groundwater in Delingha, Northwest China. J. Hydrol. 598.
Yapiyev, V., Rossi, P.M., Ala-Aho, P., Marttila, H., 2023. Stable water isotopes as an indicator of surface water intrusion in shallow aquifer wells: a cold climate perspective. Water Resour. Res. 59.
Yuan, R., Wang, M., Wang, S., Song, X., 2020. Water transfer imposes hydrochemical impacts on groundwater by altering the interaction of groundwater and surface water. J. Hydrol. 583.
Zaremehrjardy, M., Victor, J., Park, S., Smerdon, B., Alessi, D.S., Faramarzi, M., 2022. Assessment of snowmelt and groundwater-surface water dynamics in mountains, foothills, and plains regions in northern latitudes. J. Hydrol. 606.
Zhou, Z., Zhou, Z., 2023. Investigating the hydrodynamic and biogeochemical evolutions of the hyporheic zone due to large-scale reservoir impoundment. J. Hydrol. 620.